

base RNA length increase) or inhibition of the elongation step (producing transcripts shorter than 1 kb).

For the PU1 titration, the apparent midpoint for half-maximal transcription repression is  $4 \pm 2$  nM, which should approximate the  $K_d$  for triplex formation in this assay (20). The apparent  $K_d$  is approximately 100-fold lower than the corresponding value measured by footprinting or band shift analysis (Figs. 2 and 3). However, because the physical binding data were accumulated in a buffer that had not been optimized systematically (and is much simpler than the nuclear extracts, which almost certainly contain a variety of small polycations), it is likely that the  $K_d$  inferred from transcription inhibition may more clearly approximate PU1 binding affinity in a cellular context.

Although we cannot rule out all other possibilities, our physical and transcriptional data are consistent with the idea that triple-strand complex formation at the -115-bp binding site will repress transcription initiation from the human *c-myc* gene in vitro.

Considerable work remains before the structure and thermodynamics of this class of site-specific binding interaction can be fully understood. However, the PU1-*myc* complex that we have described is a useful starting point for physical and biochemical studies.

The -100 to -300 region of the human *c-myc* gene is important for transcription control in vitro (19). Also, this region is required for transcription from P1, and to a lesser extent from P2, in transient in vivo assays (21).

We propose that, although the -115-bp site may be required for activation of the *c-myc* gene (perhaps as a protein binding site), it cannot function in that way while bound to form a triplex.

It remains to be proved if triplex formation occurs in vivo. However, in some instances third-strand binding could serve as an alternative to protein binding as the physical basis for the regulation of transcription.

For technical reasons, we studied the process of using DNA oligonucleotides. However, if third-strand binding is used as a regulatory element in the cell, it is more likely that such interactions are based on endogenous RNA molecules. To stabilize such RNA with respect to hydrolysis, and as a mechanism to neutralize the unfavorable negative charge density of the triplex, it is likely that RNA molecules of this kind would exist in the cell as a protein complex. Such an RNA-protein complex might be a member of the class of small nuclear ribonucleoproteins (1) that, with the exception of

the splicing machinery, remain largely undefined.

If, among that heterogeneous family of RNA-protein particles, there are members possessing an RNA component that binds to the human *c-myc* gene by triplex formation, the binding and transcriptional analyses described here provide tools that can be used to identify them.

#### REFERENCES AND NOTES

1. P. Sharp, *Cell* **50**, 147 (1987).
2. J. Kitajewski *et al.*, *ibid.* **45**, 195 (1986).
3. G. Blobel and B. Dobberstein, *J. Cell. Biol.* **67**, 835 (1975).
4. R. J. Britten and E. H. Davidson, *Science* **165**, 349 (1969).
5. T. C. Boles and M. E. Hogan, *Biochemistry* **26**, 367 (1987).
6. S. Arnott and E. Selsing, *J. Mol. Biol.* **88**, 509 (1974).
7. S. Arnott and P. J. Bond, *Nature New Biol.* **244**, 99 (1973).
8. S. L. Broitman, D. D. Im, J. R. Fresco, *Proc. Natl. Acad. Sci. U.S.A.* **84**, 5120 (1987).
9. C. R. Cantor and P. R. Schimmel, *Biophysical Chemistry, Part I: The Conformation of Biological Macromolecules* (Freeman, San Francisco, 1980), pp. 192-195.
10. C. E. Bugg *et al.*, *Biophys. Biochem. Res. Comm.* **33**, 436 (1968); D. G. Watson, D. J. Sutor, P. Tollin, *Acta Cryst.* **19**, 111 (1965).
11. Oligonucleotides PU1 and PY1 were prepared by the phosphoramidite method on an automated synthesizer (Applied Biosystems, Inc.). Portions (1  $\mu$ g) of each oligomer were 5' end-labeled with [ $\alpha$ - $^{32}$ P]ATP and T4 polynucleotide kinase, deproteinized, and purified by means of Sephadex G25 chromatography.
12. K. L. Beattie *et al.*, *J. Mol. Biol.* **116**, 783 (1977).
13. To assay for triplex formation,  $^{32}$ P-labeled PY1 was titrated with unlabeled PU1 (in 20 mM tris-HCl, pH 7.2, 10 mM MgCl<sub>2</sub>, 10% sucrose), then loaded on a 10% polyacrylamide: 0.5% bisacrylamide gel [containing 90 mM tris-borate, pH 8.0, and 5 mM MgCl<sub>2</sub> (no EDTA)]. Electrophoresis was performed at 10 V/cm for 2 hours at 4°C. Under those conditions, kinetic analysis showed that triplex life-
14. Binding data as in Fig. 2A have been quantified by densitometry to yield the duplex/triplex ratio (D/T) as a function of the inverse of the total added PU1 strand concentration. If triplex formation approximates a simple bimolecular process, then  $D/T = K_d \times 1/[PU1]$ , where  $K_d$  is the dissociation constant. The data of Fig. 2 have been fit to this relation to yield an apparent  $K_d = 4 \pm 2 \times 10^{-7} M$ .
15. D. Rhodes and A. Klug, *Cell* **46**, 123 (1986).
16. C. Keding *et al.*, *Biochem. Biophys. Res. Comm.* **38**, 165 (1970); E. H. Postel, D. J. Norman, S. J. Flint, *Genes Dev.*, in press.
17. A. J. Berk and P. A. Sharp, *Proc. Natl. Acad. Sci. U.S.A.* **75**, 1274 (1978).
18. M. Cooney, G. Czernuszewicz, E. H. Postel, S. J. Flint, M. E. Hogan, unpublished observations.
19. J. Battey *et al.*, *Cell* **34**, 779 (1983).
20. We define *fas* equal to the transcription rate at some added oligonucleotide concentration [S], divided by that in the absence of added oligonucleotide. If transcription initiation is completely repressed by triplex formation, then transcription data should be simply related to the fraction of *myc* promoter sites that remains as a duplex. Specifically,  $(1/f) - 1 = [S]/K_d$ , where  $K_d$  is the apparent bimolecular dissociation constant for the triplex to duplex equilibrium. A regression of the PU1 titration data in Fig. 4 yields  $K_d = 4 \pm 2 \times 10^{-9} M$ .
21. N. Hay *et al.*, *Genes Dev.* **1**, 659 (1987).
22. To prepare DNA for footprinting, the plasmid pM-HX, containing the first *myc* exon and 2 kb of 5' flanking sequence (5), was cleaved with Xma I and Sca I, 3' end-labeled at its Xma I site with [ $\alpha$ - $^{32}$ P]dCTP and Klenow polymerase, then purified by means of Sepharose 4B chromatography.
23. We thank J. R. Fresco for advice and discussion in evaluating the oligomer sequences that might bind to the *myc* DNA target sequence. Supported by grants from the National Cancer Institute (M.H.) and the National Institutes of Health (S.J.F.).

27 January 1988; accepted 26 May 1988

## Large Microtubule-Associated Protein of *T. brucei* Has Tandemly Repeated, Near-Identical Sequences

ANDRE SCHNEIDER,\* ANDREW HEMPHILL, TONI WYLER, THOMAS SEEBECK†

The parasitic protozoan *Trypanosoma brucei* contains a highly organized membrane skeleton, consisting of a dense array of parallel, singlet microtubules that are laterally interconnected and that are also in tight contact with the overlying cell membrane. A high molecular weight, heat-stable protein from this membrane skeleton was isolated that is localized along the microtubules. Protease digestion experiments and sequencing of a cloned gene segment showed that most of the protein is built up by more than 50 nearly identical tandem repeats with a periodicity of 38 amino acids.

**M**ICROTUBULE-ASSOCIATED PROTEINS (MAPs) from many different organisms and tissues have been extensively studied (1-5), and their role in such cellular functions as differentiation and intracellular transport are beginning to be understood. The cytoskeleton of

A. Schneider, A. Hemphill, T. Seebeck, Institut für allgemeine Mikrobiologie, Universität Bern, CH-3012 Bern, Switzerland.  
T. Wyler, Zoologisches Institut, Universität Bern, CH-3012 Bern, Switzerland.

\*Present address: Biozentrum, Klingelbergstrasse 70, CH-4056 Basel, Switzerland.

†To whom correspondence should be addressed.

the trypanosome represents an excellent system for the analysis of MAPs involved either in microtubule-microtubule or microtubule-membrane interactions. It essentially consists of a cage of microtubules that encloses the entire cell body and is tightly apposed to the plasma membrane, such that it forms a virtual membrane skeleton (6, 7). The links between microtubules and cell membrane, as well as those between neighboring microtubules, are probably mediated by MAPs. The tubulins of trypanosomes have been studied in some detail both on the genetic (8–14) and on the biochemical level (6, 15–18). In contrast, very little is still known about the MAPs of this organism (19). We have recently identified, in the membrane skeleton of the African trypanosome *Trypanosoma brucei*, a high molecular weight, heat-resistant protein (p320) (20), and we here describe its intracellular location and its highly repetitive structure.

Structurally well defined cytoskeletons, which consist of the intact membrane skeleton cage and the flagellum, can be obtained

by extracting *T. brucei* cells in a microtubule-stabilizing buffer containing Triton X-100 (6). Further dissociation of this cytoskeleton with 0.75M NaCl solubilizes the membrane skeleton, while the flagellum remains intact and can be removed by centrifugation. Upon heat treatment of the solubilized membrane skeleton components, the large majority of the proteins are precipitated. The remaining heat-resistant protein fraction is highly enriched for p320, which migrates in SDS gel electrophoresis with an apparent molecular size of about 320 kD. This protein was purified by preparative SDS gel electrophoresis and was then used to raise polyclonal antibodies in rats (anti-p320). The antibodies were affinity-purified on nitrocellulose-bound p320 (21) before use.

For immuno-electron microscopy, cytoskeletons were prepared with buffers lacking divalent cations. This treatment induced partial disintegration of the cytoskeletons, which resulted in better spreading on the carbon film and in improved accessibility for

anti-p320 (Fig. 1A). The microtubules, which were visualized by uranyl acetate contrast staining, appeared uniformly labeled indicating that p320 was localized along their entire length. To further confirm this co-localization, specimens were also doubly stained, by means of rat antibody against p320 and a rabbit antibody against tubulin. The two could be distinguished by means of appropriate second antibodies labeled with 15-nm or 5-nm colloidal gold (Fig. 1B). Co-localization of tubulin and p320 in the microtubules was observed, which is in agreement with the observation that p320

**Fig. 1.** Ultrastructural localization of p320 in the membrane skeleton of *T. brucei*. (A) Immunogold labeling of trypanosomal cytoskeletons with anti-p320 and a second antibody (goat anti-rat IgG) conjugated to 15 nm of colloidal gold. (B) Double labeling of cytoskeletons with anti-p320 (second antibody conjugated to 15-nm colloidal gold) and anti-tubulin (goat anti-rabbit IgG as second antibody conjugated to 5-nm gold). (C) Labeling of cytoskeletons with anti-p320 affinity-purified on a  $\beta$ -galactosidase/p320 fusion protein, and goat anti-rat IgG conjugated to 15-nm colloidal gold. Bar, 5  $\mu$ m. For immunogold labeling, polyclonal anti-MARP serum raised in rats and a polyclonal anti-tubulin serum raised in rabbits were used. Antibodies were affinity-purified by adsorption to nitrocellulose strips containing the corresponding antigens (22). Gold-labeled second antibodies were purchased from Janssen Life Science Products. The  $\beta$ -galactosidase/p320 fusion protein was prepared from the lysogenic bacterial strain ( $\lambda$  TbmARP 1.1) and antibodies against it were affinity-purified as outlined above. Cytoskeletons were prepared as described (6) and were then resuspended in MEE buffer plus 0.1% glutaraldehyde and incubated on ice for 5 to 10 min. Fixed cytoskeletons were loaded onto carbon-coated nickel grids. All further incubations were done in 20 mM tris-buffer, pH 8.2. Grids were washed twice for 5 min with tris-buffer containing 1% NaBH<sub>4</sub>. Before applying the first antibody, the grids were incubated twice for 10 min in tris-buffer containing 0.1% bovine serum albumin. Staining with the first antibody was done in the same buffer for 2 to 4 hours (for double labeling, both antibodies were applied at the same time). Grids were washed five times for 5 min in tris-buffer and were then incubated with the second antibody diluted 1:5 in tris-buffer containing 0.1% bovine serum albumin for 2 to 4 hours. The subsequent washing was done as before. After postfixing the grids 5 min in tris-buffer containing 1% glutaraldehyde and two additional washing steps, they were negatively-stained with 1M uranyl acetate.

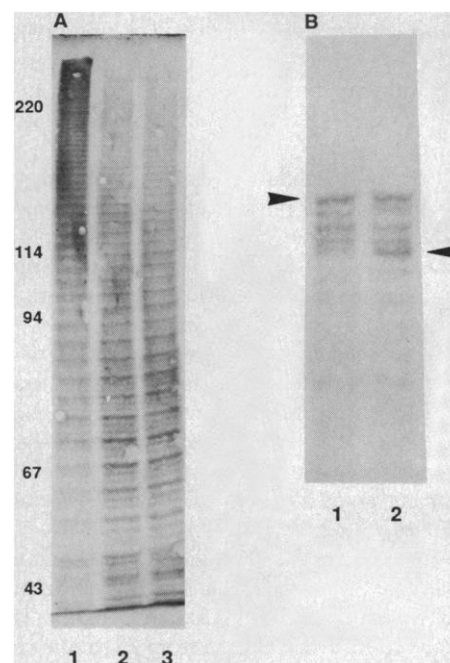
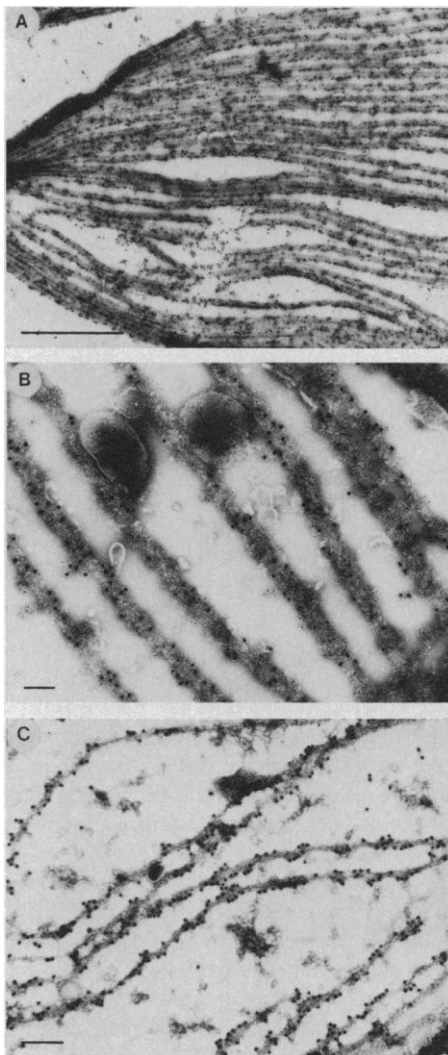


**Fig. 2.** Distinct proteolytic patterns of p320 and a  $\beta$ -galactosidase/p320 fusion protein. (A) Total heat-stable cytoskeletal proteins (see below) were incubated for 0, 5, and 10 min at room temperature (lanes 1 to 3), fractionated by gel electrophoresis and transferred to nitrocellulose. The p320 was visualized by immunostaining with anti-p320 serum. (B) Immunoblot of  $\beta$ -galactosidase/p320 fusion protein incubated either with Triton X-100 supernatant of trypanosomes (lane 1) or with chymotrypsin (lane 2) as detailed below. The positions of intact  $\beta$ -galactosidase/p320 fusion protein (upper arrowhead) and of  $\beta$ -galactosidase (lower arrowhead) are indicated. Preparation of trypanosomal heat-stable cytoskeleton proteins was essentially done as described for brain (30, 31). Briefly, cytoskeletons (6) were suspended in MME buffer containing 0.75M NaCl, incubated for 10 min in ice, and then centrifuged for 10 min at 16,000g. The supernatant containing solubilized cytoskeletal proteins was boiled for 5 min, quenched in ice, and centrifuged at 100,000g for 20 min. The supernatant from this step is referred to as the heat-stable cytoskeletal proteins. This fraction is highly enriched for p320. For protease digestion experiments, 4  $\mu$ g of fusion protein were incubated either in 2 ml of Triton X-100 supernatant obtained from  $5 \times 10^8$  trypanosomes, or with 2 ng of chymotrypsin (Fluka) in a volume of 50  $\mu$ l. Both reactions were incubated for 20 min at 37°C.

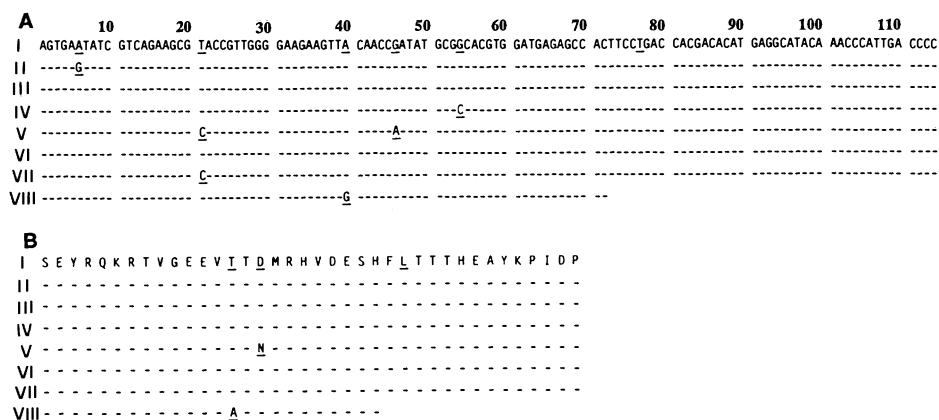


**Fig. 3.** Nucleotide and corresponding amino acid sequence of the genomic DNA insert in clone 1/1. (A) The trypanosomal DNA sequence contained in the recombinant phage  $\lambda$ TbMARP 1.1 (see legend to Fig. 1) was determined. The nucleotide sequence of the first repeat is given on the first line; for the seven following repeats only nucleotide substitutions are shown. Roman numerals indicate the different repeat units. (B) Derived amino acid sequences. The DNA insert of the lambda phage was subcloned into the Bluescript vector (Stratagene). Ordered deletions were produced by a combination of exonuclease and mung bean nuclease digestions, following the procedures given in the Stratagene manual. Sequencing was performed using the Sequenase kit (U.S. Biochemical Corp.), following the instructions of the manufacturer.

copolymerizes with tubulin upon taxol-induced microtubule formation from trypanosomal cell lysates (22). These criteria indicate that p320 is indeed a component of the microtubules of the trypanosomal membrane skeleton.

Only microtubules of the membrane skeleton, but not those of the axoneme, were stained by the antibody and therefore carry the bound protein. By contrast, a glycosomal protein (p60) which was able to stick to microtubules upon detergent extraction of the cells (22a) was found to be bound nonspecifically both to the cell body and the flagellum.

The anti-p320 was used to isolate fragments of the corresponding gene from a genomic gt11 library of *T. brucei* STIB 366. From the immunopositive phages, one phage containing a 0.9-kb insert of trypanosomal DNA was selected ( $\lambda$  TbMARP 1.1), a lysogen was constructed, and the  $\beta$ -galactosidase/p320 fusion protein was isolated. The anti-p320 was affinity-purified on this fusion protein; the affinity-purified antibody was still able to recognize p320 in immunoblot experiments. This affinity-purified antibody was then again used for immunoelectron microscopy (Fig. 1C). Antibodies prepared by affinity purification either to authentic p320 or to the  $\beta$ -galactosidase/p320 fusion protein produced essentially the same staining pattern on the microtubules.

Initial attempts to purify p320 from cytoskeletons met with great difficulties because of its high protease sensitivity. Whenever proteolysis occurred during extraction, a distinct repeating triplet pattern was observed, consisting of one strong band and two weaker ones, with an apparent size

difference between adjacent triplets of about 5 kD (Fig. 2A). This pattern was detected by affinity-purified antibodies against p320 or against the  $\beta$ -galactosidase fusion protein, and also by a monoclonal antibody (2F4) raised against p320. Upon incubation at room temperature for 5 to 10 min (lanes 2 and 3), a slight shift of the pattern toward smaller fragments was observed, although the unit size remained unaltered. This degradation was presumably caused by one or more endogenous proteases, since the conditions of extraction strongly influence the extent of proteolysis obtained. On many blots, more than 50 such triplets could be discerned, though many more were still present in the higher molecular weight range of the gel, but could not be clearly identified for lack of resolution. This striking pattern of proteolysis suggested a highly repeated internal structure of p320 and indicated that it should comprise the major part of this protein.

To determine if the characteristic pattern of proteolysis was due to the primary amino acid sequence or to structural properties or protein-protein interactions in situ, the  $\beta$ -galactosidase/p320 fusion protein was analyzed for the potential occurrence of similar proteolytic fragments. The fusion protein was incubated either with a Triton X-100 extract from trypanosomes, which contains much of the protease activity responsible for p320 degradation, or with chymotrypsin (Fig. 2B). In both cases, the digestion resulted in a pattern of regularly spaced bands of decreasing size, again with a spacing of about 5 kD. The largest of these bands corresponded to the intact fusion protein, while the lowest band comigrated with the  $\beta$ -galactosidase marker. This result indicates

that under the conditions used, the  $\beta$ -galactosidase part of the fusion protein was not digested, while the trypanosomal part was degraded to a similar fragment pattern as was found with endogenous p320. These observations strongly indicate that this characteristic proteolysis pattern is due to structural properties of p320 that are maintained in the bacterially synthesized protein, and hence most likely were due to features of the primary amino acid sequence.

This view was confirmed by nucleotide sequence analysis of the 0.9-kb p320 gene fragment from the recombinant phage  $\lambda$  TbMARP 1.1. Its entire DNA sequence consists of highly conserved, tandemly arranged repeats (Fig. 3). Out of 870 nucleotides sequenced, exchanges have occurred at only six positions (0.7%). The repetitive sequence was not cleaved by many tetranucleotide restriction enzymes (for example, Dpn I, Hae III, Hpa II, Mbo I, Nde II, Pal I, Sau 3A, Tag I, Mae I, Msp I, and Tha I). When genomic trypanosomal DNA is digested with several such enzymes, the p320 gene remains on a high molecular weight fragment (21), indicating that a very large proportion of the gene consists of the conserved 114-bp repeat. The amino acid sequence consists of tandemly repeated, highly conserved blocks of 38 amino acids. Among the 290 amino acids, only two (0.7%) exchanges have occurred. Secondary structure predictions indicate that each repeat unit may contain a  $\alpha$ -helical region of about 20 amino acids (out of 38 amino acids per repeat unit) extending from positions 12 to 31 (Fig. 3). Thus, p320 may assume an elongated, highly regular configuration where helical segments alternate with non-helical segments of similar length. The proteolysis patterns (Fig. 2A) indicate that a very large proportion of the molecule may assume this repetitive configuration, a suggestion that agrees with genomic blotting experiments.

Our results establish that a major microtubule-associated protein from the membrane skeleton of *T. brucei* is a highly repetitive structure consisting of strongly conserved, tandemly arranged blocks of 38 amino acids in length. This is an unexpected finding for a cytoskeletal protein inasmuch as most other highly repetitive proteins found so far are either secreted or exposed on the cell surface (23–27). Protease digestion experiments, surface labeling with radioactive iodine, and immunofluorescence staining of the outer cell surface have ruled out the possibility that p320 is on the cell surface (20). In the best studied cytoskeletal protein in which repetitions have been found, spectrin, the degree of conservation is much lower than that found in the trypanosomal p320 (28). A

relation between p320 and mammalian high molecular weight MAPs is suggested by the observation that antibody against hog brain MAP 2 reacts weakly with trypanosomal p320, and vice versa (20). The only MAP whose complete sequence has been published so far is the tau protein of mouse brain (29). No similarity between p320 and tau primary sequence is observed. However, the tau sequence also contains three repetitive stretches of 18 amino acids. This, together with proteolysis experiments with mammalian MAP 3 (30) and direct protein sequencing of a 180-kD MAP from the spindle apparatus (31) suggest that a repetitive motive may be a common feature in MAP architecture.

## Nonoxidative Glucose Consumption During Focal Physiologic Neural Activity

PETER T. FOX,\* MARCUS E. RAICHLE, MARK A. MINTUN, CARMEN DENCE

Brain glucose uptake, oxygen metabolism, and blood flow in humans were measured with positron emission tomography, and a resting-state molar ratio of oxygen to glucose consumption of 4.1:1 was obtained. Physiologic neural activity, however, increased glucose uptake and blood flow much more (51 and 50 percent, respectively) than oxygen consumption (5 percent) and produced a molar ratio for the increases of 0.4:1. Transient increases in neural activity cause a tissue uptake of glucose in excess of that consumed by oxidative metabolism, acutely consume much less energy than previously believed, and regulate local blood flow for purposes other than oxidative metabolism.

### REFERENCES AND NOTES

1. J. B. Olmsted, *Annu. Rev. Cell Biol.* **2**, 421 (1986).
2. L. Pillus and F. Solomon, *Proc. Natl. Acad. Sci. U.S.A.* **83**, 2468 (1986).
3. L. S. Goldstein, R. A. Laymon, R. J. McIntosh, *J. Cell Biol.* **102**, 2076 (1986).
4. G. Wiche, *Trends Biochem. Sci.* **10**, 67 (1985).
5. R. B. Vallec, *Cell Muscle Motility* **5**, 289 (1984).
6. A. Schneider *et al.*, *Cell Biol.* **104**, 431 (1987).
7. E. Angelopoulos, *J. Protozool.* **17**, 39 (1970).
8. J. Wu and L. R. Yarbrough, *Gene* **61**, 51 (1987).
9. M. A. Imboden, P. Laird, M. Affolter, T. Seebeck, *Nucleic Acids Res.* **15**, 7357 (1987).
10. S. Sather and N. Agabian, *Proc. Natl. Acad. Sci. U.S.A.* **82**, 5695 (1985).
11. M. A. Imboden, B. Blum, T. De Lange, R. Braun, T. Seebeck, *J. Mol. Biol.* **188**, 393 (1986).
12. B. E. Kimmel *et al.*, *Gene* **35**, 237 (1985).
13. L. S. Thomashow *et al.*, *Cell* **32**, 35 (1983).
14. T. Seebeck *et al.*, *Proc. Natl. Acad. Sci. U.S.A.* **80**, 4634 (1983).
15. T. Sherwin *et al.*, *J. Cell Biol.* **104**, 439 (1987).
16. M. T. Dolan, C. G. Reid, H. P. Voorheis, *J. Cell Sci.* **80**, 123 (1986).
17. D. G. Russell, D. Miller, K. Gull, *Mol. Cell. Biol.* **4**, 779 (1984).
18. J. Stieger *et al.*, *J. Biol. Chem.* **259**, 4596 (1984).
19. T. Seebeck, V. Küng, T. Wyler, M. Müller, *Proc. Natl. Acad. Sci. U.S.A.* **85**, 1101 (1988); G. T. Bramblett, S. Chang, M. Flavin, *ibid.* **84**, 3259 (1987); C. G. Jensen and B. W. Smail, *Ann. N.Y. Acad. Sci.* **466**, 417 (1986).
20. A. Hemphill *et al.*, in preparation.
21. A. Schneider, unpublished data.
22. J. B. Olmsted, *J. Biol. Chem.* **256**, 11955 (1981).
- 22a. V. Kueng, A. Schlaeppli, T. Seebeck, in preparation.
23. M. R. Mowatt and C. E. Clayton, *Mol. Cell. Biol.* **7**, 2828 (1987).
24. I. Roditi *et al.*, *Nature* **325**, 272 (1987).
25. D. S. Peterson, R. A. Wrightsman, J. E. Manning, *ibid.* **322**, 566 (1986).
26. A. F. Cowman *et al.*, *Cell* **40**, 775 (1985).
27. M. A. T. Muskawitch and D. S. Nogness, *ibid.* **29**, 1041 (1982).
28. D. W. Speicher and V. Marchesi, *Nature* **311**, 177 (1984).
29. G. Lec, N. Cowan, M. Kirschner, *Science* **239**, 285 (1988).
30. G. Huber, D. Alaimo-Beuret, A. Matus, *J. Cell Biol.* **100**, 496 (1985).
31. G. Maier *et al.*, *Biol. Chem. Hoppe-Seyler* **368**, 440 (1987).
32. W. Herzog and K. Weber, *Eur. J. Biochem.* **92**, 1 (1987).
33. A. Fellous, J. Frances, A. M. Lemmon, J. Nunez, *Eur. J. Biochem.* **78**, 167 (1977).
34. We thank U. Kurath for excellent technical support; N. Mueller for advice and discussions; R. Braun, G. Wiche, T. Kreis, and A. Matus for comments on the manuscript; and G. Wiche for polyclonal antibody against porcine MAP 2. Supported by grant Nr 3.580-1.87 of the Swiss National Science Foundation.

UNDER NORMAL CONDITIONS, THE brain's energy demands [adenosine triphosphate (ATP) production] are thought to be provided almost exclusively by glucose oxidation. For the resting state, this idea is well established (1). More than 90% of all resting-state glucose consumption is oxidative, with 5% (or less) being metabolized to lactate. Because of the efficiency of oxidation (at least 15 times more ATP yield than glycolysis), more than 99% of the ATP production in resting tissue is by glucose oxidation. The phasic energy demands accompanying physiological increases in neural activity, however, are less well studied. Local cerebral glucose metabolic rate (CMRglu) and cerebral blood flow (CBF) are greatly increased by focal increases in neural activity. The increase in CMRglu has been thought to indicate a local increase in glucose oxidation, supporting large energy expenditures required to maintain membrane ionic gradients. The increase in local CBF has been considered a response to substrate (O<sub>2</sub>) depletion and metabolite (CO<sub>2</sub>) excess.

Challenging the conventional formulation, we reported that a focal, physiological increase in neural activity induced by peripheral tactile stimulation increased cerebral metabolic rate for O<sub>2</sub> (CMRO<sub>2</sub>) minimally (5%), despite a large increase (29%) in local CBF (2). To confirm and extend these observations we measured the CMRglu, CMRO<sub>2</sub>, and CBF of human visual cortex at rest and during visual stimulation.

All measurements were doubly paired; each volunteer (3) had blood flow and metabolic rate measured in both the stimulated and the unstimulated state during a single scanning session. The CBF and CMRO<sub>2</sub> were measured in one five-subject group (4); CBF and CMRglu were measured in a second five-subject group (5). Control-state measurements were made with the subject's

eyes closed. Stimulated-state measurements were made as the subject viewed an annular reversing checkerboard (6). Cortical responses in primary visual cortex were identified with images of regional change (Figs. 1 and 2) created by superposition and subtraction (stimulus minus control) of intrasubject pairs of images for each subject and each variable.

In the resting state, the mean whole-brain (7) CMRO<sub>2</sub> and CMRglu were 1.50 ± 0.071 (SD) and 0.37 ± 0.053 μmol min<sup>-1</sup> 100 g<sup>-1</sup>, respectively. This is a 4.1:1 molar ratio, in good agreement with published values (1, 8). The same resting-state molar ratio (4.1:1) was present in primary visual cortex, where CMRO<sub>2</sub> and CMRglu were 1.71 ± 0.183 and 0.42 ± 0.033 μmol min<sup>-1</sup> 100 g<sup>-1</sup>, respectively. As expected, a strong resting-state regional correlation between CBF and metabolism (CMRO<sub>2</sub> and CMRglu) was evident from simple visual inspection of their regional distributions (Figs. 1 and 2). Moreover, multiregional (7) correlations of CMRO<sub>2</sub> and CBF (n = 5) and of CMRglu and CBF (n = 5) were significant (P < 0.0001) in all cases.

In every subject the CMRglu and CBF of visual cortex were markedly increased by visual stimulation (Table 1), rising a mean of 0.21 μmol min<sup>-1</sup> 100 g<sup>-1</sup> (51%) and 27 ml min<sup>-1</sup> 100 g<sup>-1</sup> (50%), respectively (Table 1 and Fig. 1). However, CMRO<sub>2</sub> increased only a mean of 0.08 μmol min<sup>-1</sup> 100 g<sup>-1</sup> (5%) (Table 1 and Fig. 2), in accord with our observations in somatosensory cortex (2, 9). The molar ratio for the increase in metabolic rate was only 0.4:1 (O<sub>2</sub>:glucose). Thus, 91% of the activity-induced increase in glucose uptake was not oxidized.

Division of Radiation Sciences, Mallinckrodt Institute of Radiology, Washington University School of Medicine, St. Louis, MO 63110.

\*To whom correspondence should be addressed.